

## Supplementary Information

### Drop mobility on superhydrophobic microstructured surfaces with wettability contrasts

Yutaku Kita<sup>1,2</sup>, Coinneach Mackenzie Dover<sup>3</sup>, Alexandros Askounis<sup>4</sup>, Yasuyuki Takata<sup>1,2</sup>, and Khellil Sefiane<sup>\*3</sup>

1. Department of Mechanical Engineering, Kyushu University, 744 Motooka, Nishi-ku, Fukuoka, 819-0395, Japan
2. International Institute for Carbon-Neutral Energy Research (WPI-I<sup>2</sup>CNER), Kyushu University, 744 Motooka, Nishi-ku, Fukuoka
3. School of Engineering, The University of Edinburgh, King's Buildings, Robert Stevenson Road, Edinburgh EH9 3FB, United Kingdom
4. Engineering, Faculty of Science, The University of East Anglia, Norwich Research Park, Norwich NR4 7TJ, United Kingdom

\*Corresponding author: K.Sefiane@ed.ac.uk

## Drop behaviour

Herein, we present the data from the rest of our experiments from our manuscript. In Fig. S1, we show the displacements of the contact points (front-red, middle-green and rear-blue) along representative snapshots, corresponding to Fig. 3. As reported in the manuscript, sequential wetting/dewetting events of the drops were observed for every case and the drops proceeded to the surfaces with larger  $\phi$  (hence, lower  $\theta_{app}$ ) mainly during the dewetting events. For the wettability contrasts with relatively small  $\Delta\phi$  i.e. Fig. S1 (a)–(c), during the dewetting events both front and rear contact points retreated significantly, although front one moved less, which resulted in small displacements during each event. In contrast, the cases depicted in the cases panels (d)–(g) in Fig. S1, exhibit wettability contrasts with large  $\Delta\phi$  and closely resemble the Sq-10-40/Sq-10-20 case shown in Fig. 3 of the manuscript. In particular, the front contact points were almost pinned during the dewetting stages, giving rise to large velocities. If both sides of the contrasts rested on large  $\phi$  shown in Fig. S1 (h)–(i) within the red box, motion of the contact points was weak and both sides were nearly pinned after the first wetting event, which resulted in significantly slower drop velocity corresponding to the red-boxed data in Fig. 4.

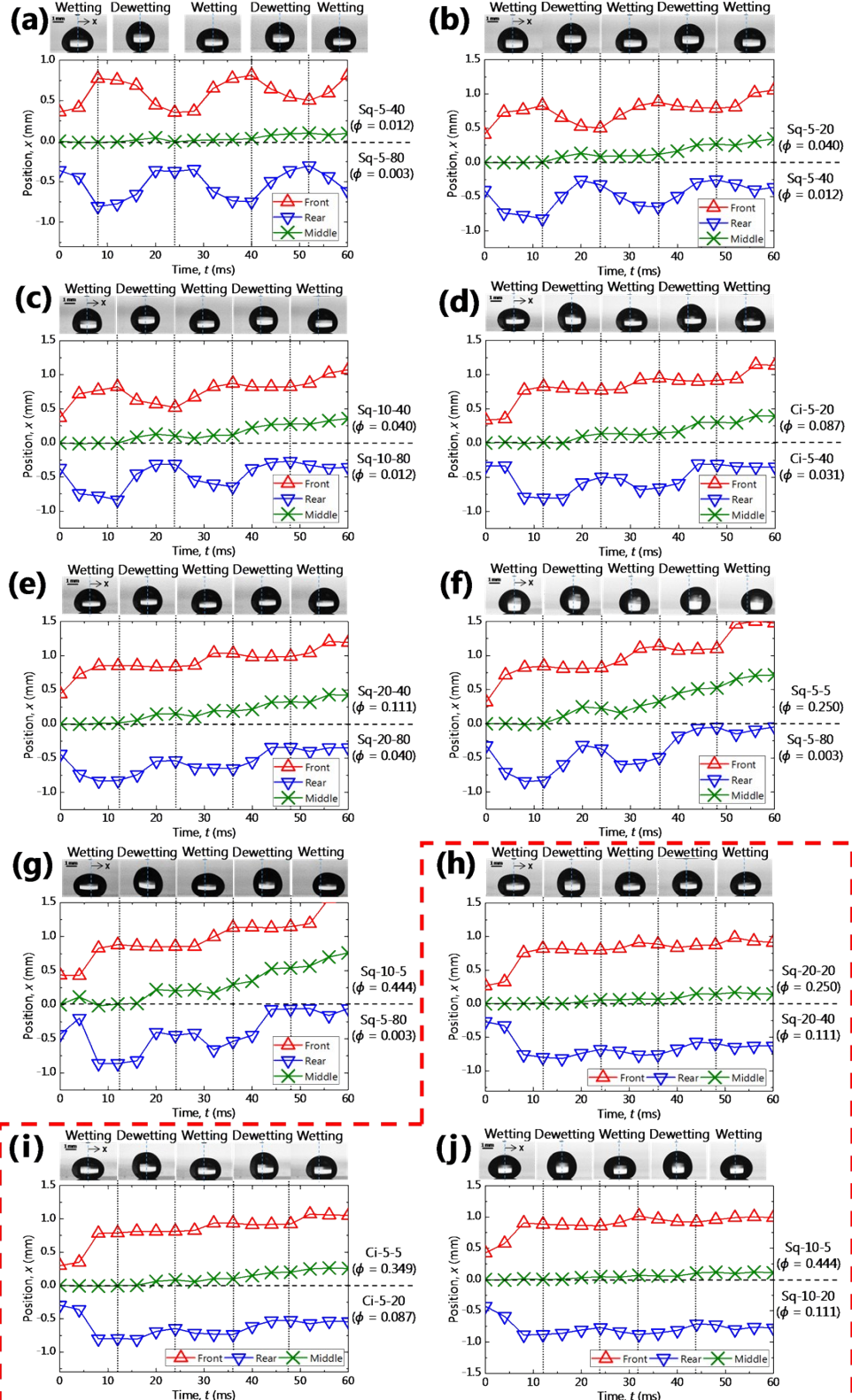


**Fig. S1** Evolution of each contact point (front, rear and middle) over time for the cases of (a) Sq-5-80/Sq-5-40, (b) Sq-5-40/Sq-5-20, (c) Sq-10-80/Sq-10-40, (d) Ci-5-40/Ci-5-20, (e) Sq-20-80/Sq-20-40, (f) Sq-5-80/Sq-5-5, (g) Sq-5-80/Sq-10-5, (h) Sq-20-40/Sq-20-20, (i) Ci-5-20/Ci-5-5 and (j) Sq-10-20/Sq-10-5. The position of the boundary is set as  $x = 0$  mm. Insets represent typical drop shape during wetting and dewetting events. The cases for slow drops corresponding to Fig. 4 are indicated in the red box.

## Surface free energy and energy diagram

In Fig. S2, we present in left column the calculated free energy evolution over time and the corresponding quantification of the energy requirements for motion for each drop/case above.

In every case, the drops minimised their energy and moved toward the surfaces with lower energy as discussed in the manuscript. The cases of Fig. S2 (h)–(j) showed significantly smaller drop velocities as in Fig. 4 of the manuscript, due to the fact that the drops at the wettability contrasts (metastable) must traverse significantly high peaks of  $G_{CAH}$  compared to other cases. Hence, we may stipulate at this point that large portion of  $G_{ini}$  was consumed to overcome the CAH, retarding motion.

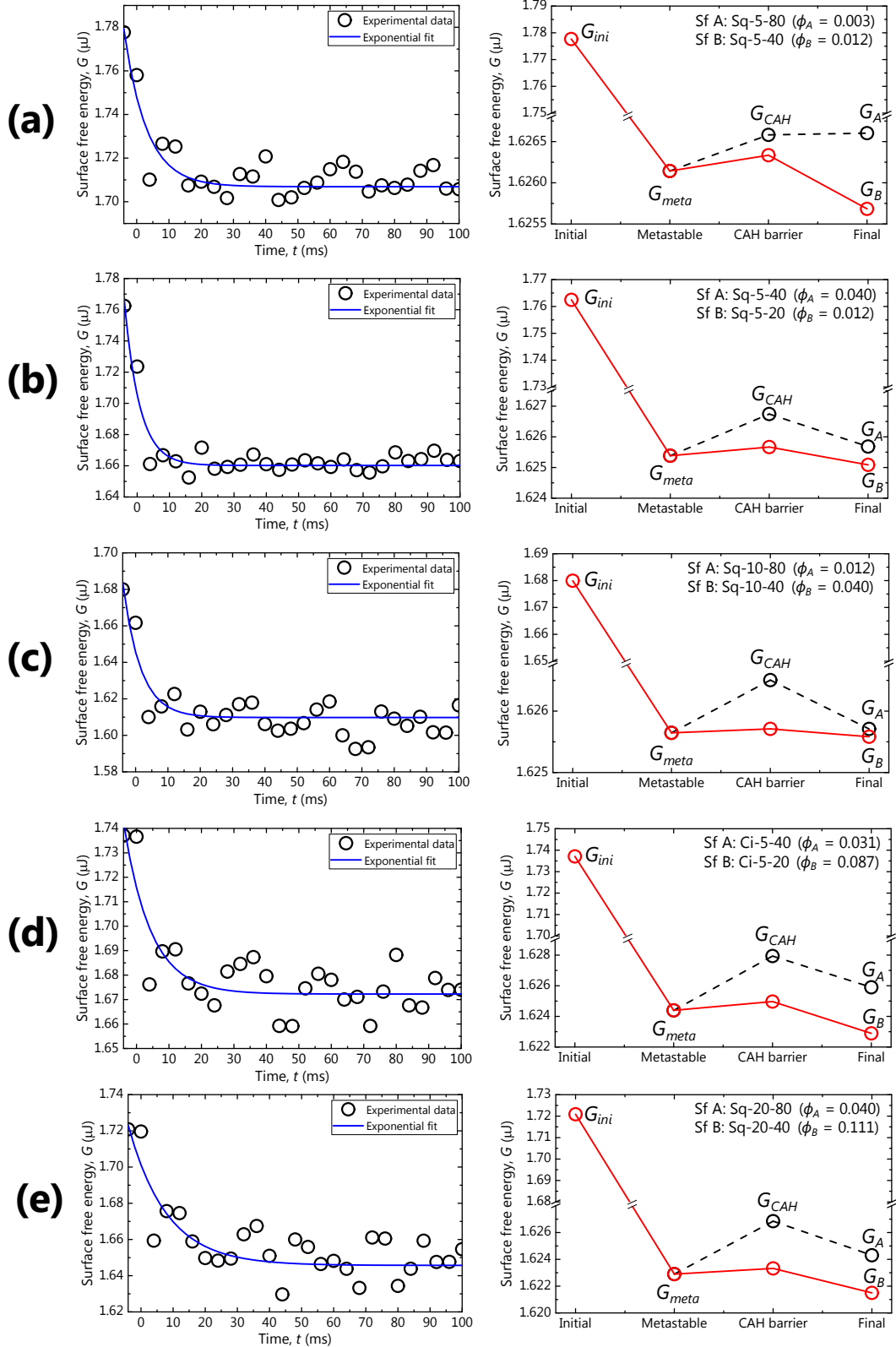


**Fig. S2** Evolution over time of the surface free energy of a drop placed at the boundaries (left column) and energy diagrams (right column) for (a) Sq-5-80/Sq-5-40, (b) Sq-5-40/Sq-5-20, (c) Sq-10-80/Sq-10-40, (d) Ci-5-40/Ci-5-20, (e) Sq-20-80/Sq-20-40, (f) Sq-5-80/Sq-5-5, (g) Sq-5-80/Sq-10-5, (h) Sq-20-40/Sq-20-20, (i) Ci-5-20/Ci-5-5 and (j) Sq-10-20/Sq-10-5. The cases for slow drops corresponding to Fig. 4 are indicated in the red box.

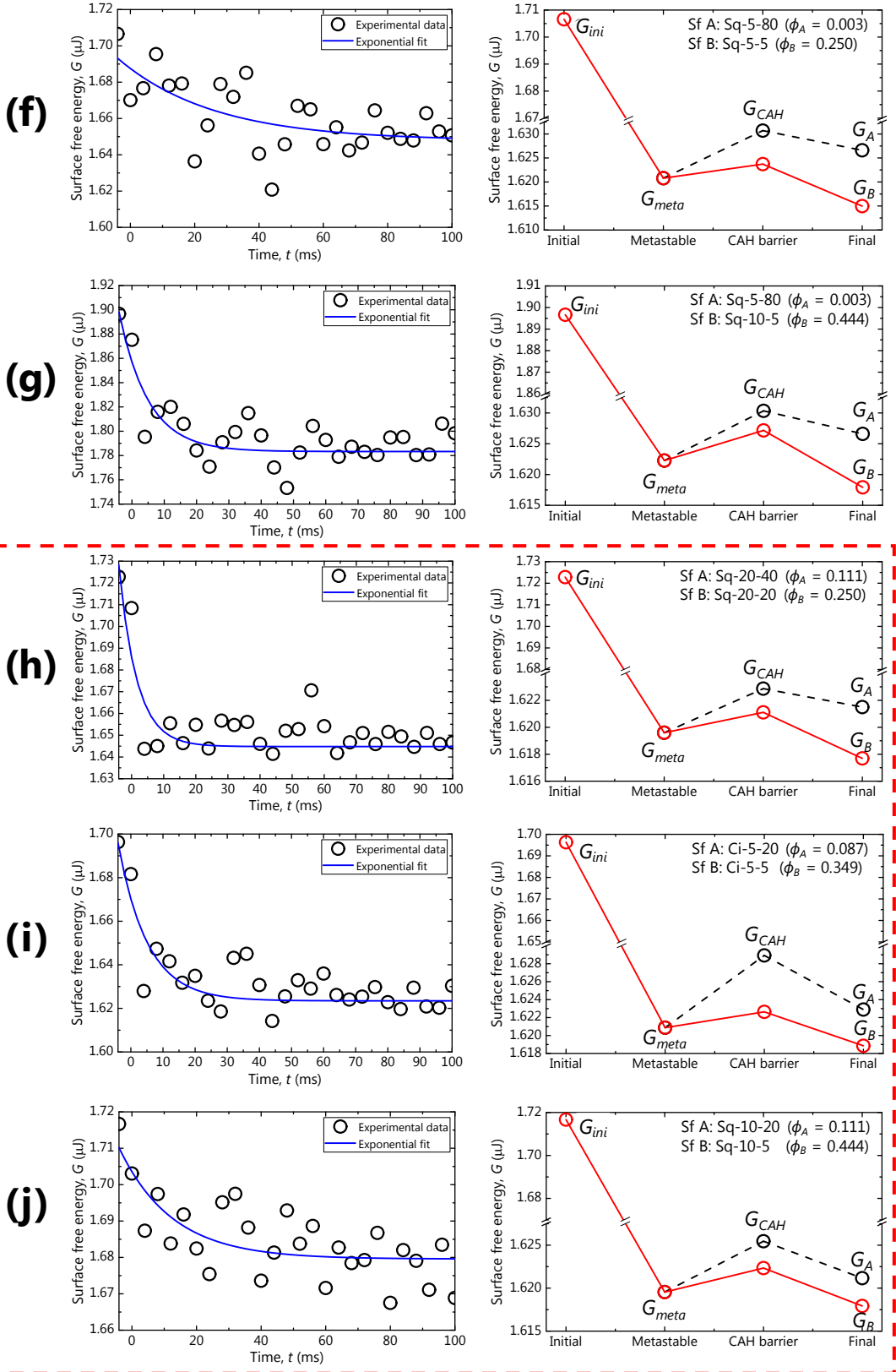


**Fig. S2 Continued.**